coatings

MDPI

Article

The Role of Electric Pressure/Stress Suppressing Pinhole Defect on Coalescence Dynamics of Electrified Droplet

Jaehyun Lee [1], Ehsan Esmaili [2,3], Giho Kang [1], Baekhoon Seong [1], Hosung Kang [2], Jihoon Kim [4], Sunghwan Jung [2,3], Hyunggun Kim [5,*] and Doyoung Byun [1,*]

1 Department of Mechanical Engineering, Sungkyunkwan University, 2066 Seoburo, Suwon 16419, Korea; pitts08@skku.edu (J.L.); kghost1030@gmail.com (G.K.); baek.hoon.seong@gmail.com (B.S.)
2 Department of Biomedical Engineering and Mechanics, Virginia Tech, Blacksburg, VA 24061, USA; ee287@cornell.edu (E.E.); intheskyaaa@gmail.com (H.K.); sunnyjsh@gmail.com (S.J.)
3 Department of Biological and Environmental Engineering, Cornell University, Ithaca, NY 14853, USA
4 Coastal & Ocean Engineering Division, Korea Institute of Ocean Science and Technology, 385 Haeyang-ro, Busan Metropolitan City 49111, Korea; jihoonkim@kiost.ac.kr
5 Department of Biomechatronic Engineering, Sungkyunkwan University, 2066 Seoburo, Suwon 16419, Korea
* Correspondence: hkim.bme@skku.edu (H.K.); dybyun@skku.edu (D.B.); Tel.: +82-31-290-7821 (H.K.); +82-31-299-4846 (D.B.)

Abstract: The dimple occurs by sudden pressure inversion at the droplet's bottom interface when a droplet collides with the same liquid-phase or different solid-phase. The air film entrapped inside the dimple is a critical factor affecting the sequential dynamics after coalescence and causing defects like the pinhole. Meanwhile, in the coalescence dynamics of an electrified droplet, the droplet's bottom interfaces change to a conical shape, and droplet contact the substrate directly without dimple formation. In this work, the mechanism for the dimple's suppression (interfacial change to conical shape) was studied investigating the effect of electric pressure. The electric stress acting on a droplet interface shows the nonlinear electric pressure adding to the uniform droplet pressure. This electric stress locally deforms the droplet's bottom interface to a conical shape and consequentially enables it to overcome the air pressure beneath the droplet. The electric pressure, calculated from numerical tracking for interface and electrostatic simulation, was at least 10^8 times bigger than the air pressure at the center of the coalescence. This work helps toward understanding the effect of electric stress on droplet coalescence and in the optimization of conditions in solution-based techniques like printing and coating.

Keywords: droplet coalescence; spray coating; charged droplet; pinhole defect; air film layer

Citation: Lee, J.; Esmaili, E.; Kang, G.; Seong, B.; Kang, H.; Kim, J.; Jung, S.; Kim, H.; Byun, D. The Role of Electric Pressure/Stress Suppressing Pinhole Defect on Coalescence Dynamics of Electrified Droplet. *Coatings* **2021**, *11*, 503. https://doi.org/10.3390/coatings11050503

Academic Editor: Ioannis Karapanagiotis

Received: 2 April 2021
Accepted: 18 April 2021
Published: 25 April 2021

1. Introduction

The coalescence of a droplet is one of the fundamental fluid dynamic phenomena that commonly occur in nature [1–3]. It is also widely utilized in various industrial applications from droplet-based microfluidic chips [4–6] to printing [7–12] and spray coating [13–16]. Generally, the prime factors affecting the coalescence behavior are (1) the physical properties of the droplets, (2) the inertia force, and (3) the characteristics of a coalescence interface. Furthermore, the additional external conditions (multi-physics such as thermodynamics or electromagnetics) also can affect the coalescence behaviors and sometimes create unexpected phenomena. For this reason, many studies on droplet coalescence under a multi-physics condition have been reported diversely until nowadays. Indeed, many industries are ceaselessly adopting various multiphysics conditions to control droplet/liquid precisely. However, our knowledge is still insufficient to predict and control all droplet coalescence phenomena that could be happened under new or various multiphysics conditions in industries. Thus, even though droplet coalescence is universally observable and has been researched for a long time, we cannot stop emphasizing the importance of continuous studies on novel droplet coalescence.

The air film is one of the phenomena that can be observed in droplet's coalescence process. Generally, right before the droplet's coalescence, the dimple is formed by the local pressure inversion near the bottom apex of the droplet interface [17,18]. The air film appears via the momentary entrapment inside the dimple. This air film can be dissipated by draining outward during coalescence or it can be entrapped as a bubble inside the coated liquid layer. Recently, it has received attention not only as the permanent bubble entrapment, but also as one of the significant factors that could affect the secondary dynamics of droplets after coalescence or the final coated film. For example, Jolet de Ruiter et al. observed that the water droplet can bounce upon the hydrophilic surface due to the mediated thin air film like the case upon a super-hydrophobic surface [19]. They showed that, through the force balance analysis, the thin air film via the dimple affects the droplet's bouncing regardless of the surface's wettability. Furthermore, in industrial technologies such as a solution-based process, e.g., printing or spray coating, the air film caused by the dimple can reduce the mechanical adhesion of the deposited layer or be an obstacle such as a pinhole defect to hinder electrical/chemical performance of the device [20–22]. To sum up, irrespective of the field that the droplet coalescence happens, the air film (dimple) becomes a significant factor that cannot be ignorable in droplet coalescence.

Meanwhile, the solution-based processes conducted under electric fields such as electrohydrodynamic jet printing or electrospray coating have shown uniform deposition with few defects (pinholes) [23–25]. However, except for the reports describing an overall observation of the quality of the final product, processed under an electric field, few studies have reported a thorough investigation of the fundamental mechanisms physically or visualizations of this phenomenon [26–28]. Recently, Deng and his coworkers reported the influence of a weak electric charge of a droplet on the impact dynamics [29]. In their report, when the electric charge on the droplet is above the critical level (1% of the Rayleigh limit), the droplet impact in a form of a conical tip resulting in contact without building up the air film layer. However, more fundamentally, the droplet's interfacial change depends on correlations of the inertial force, surface tenson, and electric stress.

Thus, in this study, we concretely elucidated the mechanism for dimple suppression due to conical interfacial shape, utilizing electric pressure (P_{electric}). Electric pressure can be compared with the air pressure at the bottom of the droplet. The effect of the electric field and electrical charge on dimple suppression was investigated under a broad range of Weber numbers (*We*). We also investigated the critical electric Weber number where the dimple starts to be suppressed. This study will help understanding of the coalescence behaviors of droplet in the micro/nanoscale and develop a more precisely controllable solution-based process.

2. Materials and Methods

2.1. Materials and Experimental Setup for Visulization of Droplet Coalescence

The ethanol and deionized (DI) water droplets were ejected by a stainless nozzle of size 34 gauge, and a syringe pump with a constant flow rate of 5 μL/min. We utilized a free fall droplet and voltage was applied to the nozzle tip directly. A waveform generator (33220A, Agilent, Santa Clara, CA USA) was used as a power source and the generated direct current (DC) was amplified by a high voltage amplifier (Trek 10/40A-HS, Advanced Energy Industries, Inc., Denver, CO, USA). ITO (Indium Tin Oxide) glass (15 Ω/sq, Sigma-Aldrich, St. Louis, MO, USA) was selected as the substrate, allowing us to observe the interference pattern at a bottom-view and to be grounded in an electric field. The strength of the electric field was controlled by changing the dripping height between the nozzle and the substrate (Figure S1). The range of the applied voltage was from 0 to 300 V. All droplets had the same diameter regardless of the electric field intensity and dripping height under our voltage range. The diameters of ethanol and DI water droplets were 1.69 ± 0.06 mm and 1.82 ± 0.02 mm, respectively. The Weber number ($We = \rho D_0{}^2 v/\sigma$, ρ is density, D_0 is droplet diameter, v is impact velocity, and σ is surface tension) ranged between 3.9 and 75.1 in ethanol experiments, and between 0.82 and 22.5 in DI water experiment, depending on the

ejection height (See Tables S1, S2 and Figure S2). Temperature and humidity may influence considerably the electrification of the droplet and the droplet ejection from the nozzle, hence were set to 25 °C and 50%, respectively, for all experiments. Two synchronized high-speed cameras, with frame rates of 20,000 fps (Figure S1), were utilized to record the overall collision sequence of the droplet on the front side and on the bottom side. The dual-wavelength interferometry method was utilized with the lasers (λ_1 = 532 nm, λ_2 = 436 nm) to observe and measure the profile and thickness air-film layer [30]. A very small amount of fluorescent dye (below 0.5 wt.%, rhodamine B isothiocyanate, Sigma) was added to Ethanol and DI water [31]. The high-speed interferometry method is a way of utilizing the interference fringe measured by a high-speed camera [32,33]. Details of the experimental method and its conditions are described in the Supplementary Materials.

2.2. Measurement of Charge Amount on Droplet ($Q_{droplet}$)

We calculated the electric pressure induced by the charge on an electrified droplet. There are two ways to estimate or to measure the amount of the charge on the droplet (indirect measurement method and direct measurement method). In our work, we chose the direct measurement method utilizing the Faraday cup to increase the reliability of the results. The lab-made Faraday cup consists of two cylindrical mesh electrodes separated by an insulator, and it was connected to electrometer (Keithley 6517A, Cleveland, OH, USA). To make the electric field strength the same as in the real experimental setup and to make the droplet pass through the copper plate to the Faraday cup, a perforated copper plate was used as a substrate. When the electrified droplet is discharged from the nozzle and passed into the Faraday cup's inner electrode, the counter electrical net charge transfers to the electrometer from the inner electrode to satisfy its electric neutrality [34,35].

3. Numerical Analysis

3.1. Electric Pressure ($P_{electric}$)

The dimple is formed by pressure inversion at the droplet interface, and the air film is occurred by the entrapment of air inside the dimple. The pressure inversion happens when the air pressure beneath the droplet exceeds droplet pressure. For an electrified droplet under the electric field, we assumed that electric pressure is added to the droplet's pressure due to its surface charge. The added electric pressure would delay or suppress the dimple formation. Therefore, it is necessary to calculate the electric pressure and compare it with air pressure. The electric pressure could be calculated considering the morphological change of droplet interface due to electric stress. This could be achieved through solving a two-phase Navier-Stokes equation combined with Maxwell stress to track the interfacial change. However, it has subtle difficulties to correctly model the charge redistribution and calculate the change of droplet interface and external electric field distribution. Therefore, in this study, we modeled and calculated the electric pressure to explain the droplet dynamics as Equation (1). In this study, the electrical charge is assumed to be uniform at the interface before dimple formation.

$$P_{\text{electric}} = \frac{F_{\text{electric}}(r)}{A(r)} = \frac{Q_{\text{droplet}} E_z(r)}{A(r)} = \frac{1}{\pi r^2} Q_{\text{droplet}} E_z(r) \quad (1)$$

where $F_{\text{electric}}(r)$ and $A(r)$ are the electric force and the surface area beneath the droplet respectively, and r is the radial distance from the center of the collision. Q_{droplet} and E_z is the charge amount on droplet and local electric field strength at the droplet's bottom surface.

Followed by Equation (1), to calculate the electric pressure, one needs the electric field strength (E_z) along the liquid droplet surface at the moment of dimple formation as well as the amount of charge (Q_{droplet}). For the charge amount on the droplet, we utilized the charge amount in Tables 1 and 2 measured by the Faraday cup. Also, for the local electric field strength along the droplet's bottom interface, electrostatic simulation was utilized, and its details are mentioned below.

Table 1. The net charge amount to an electrified ethanol droplet.

Applied Voltage	Dripping Height							
	5 mm		10 mm		15 mm		20 mm	
V	V/m	nC	V/m	nC	V/m	nC	V/m	nC
100	20,000	0.0060	10,000	0.0052	666.67	0.0043	5000	0.0029
300	60,000	0.0185	30,000	0.0156	20,000	0.0137	15,000	0.0125

Table 2. The net charge amount to an electrified DI water droplet.

Applied Voltage	Dripping Height							
	5 mm		10 mm		15 mm		20 mm	
V	V/m	nC	V/m	nC	V/m	nC	V/m	nC
100	20,000	0.0081	10,000	0.0067	666.67	0.0056	5000	0.0052
300	60,000	0.0252	30,000	0.0212	20,000	0.0186	15,000	0.0163

3.1.1. The Gap Height When a Dimple Is Firstly Formed

Figure 1a shows a schematic of a droplet when a dimple is formed by the increased air pressure. The height ($h(0,t)$) is the distance from the bottom droplet interface to the substrate, at the center of coalescence. r is the radial axis and t is time. Figure 1b depicts the development of air film in the coalescence process. t_{first} means the time when the dimple formation firstly occurs due to the air pressure in the absence of an electric field. When dimple first occurs, the dimple height at the center of the interface can be represented as $h(0,t_{\text{first}})$. Details about the method for the numerical tracking for the interface are introduced in the next sections.

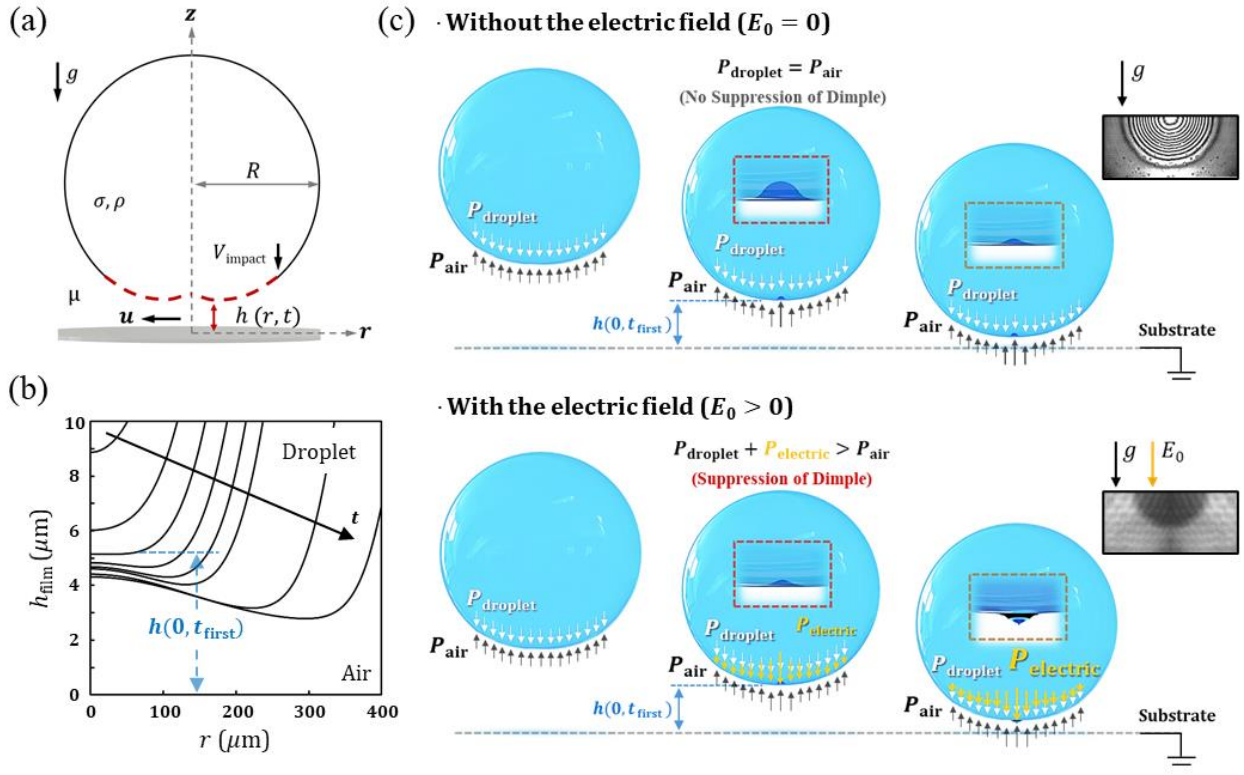

Figure 1. The suppression of a dimple (air film layer) on the electrified droplet surface. (**a**) A schematic of the droplet for numerical analysis, (**b**) The development of air film during the coalescence of a droplet and the height of interface, $h(0,t_{\text{first}})$ when a dimple is firstly formed, and (**c**) The sequence of the dimple formation and $h(0,t_{\text{first}})$ with and without electric field.

The electric pressure, caused by the electric stress on an electrified droplet, acts in an outward (normal) direction. As shown in Figure 1c (upper image), in the absence of an electric field ($E_0 = 0$), the dimple is formed by the pressure inversion at the height of $h(0, t_{\text{first}})$, where the air pressure in the gap balances with the droplet pressure ($P_{\text{droplet}} = P_{air}$ at $h(0, t_{\text{first}})$). On the other hand, for the electrified droplet under the electric field (Figure 1c, lower image), the Maxwell electric stress also affects the droplet interface. The electric pressure (P_{electric}) is augmented to the droplet internal pressure. At the height $h(0, t_{\text{first}})$, if those augmented electric pressures are stronger than air pressure ($P_{\text{droplet}} + P_{\text{electric}} > P_{\text{air}}$), the dimple formation could be suppressed or delayed. Therefore, it is necessary to calculate the electric pressure at the height of $h(0, t_{\text{first}})$.

- Governing Equations

To calculate the height, $h(0, t_{\text{first}})$, where the dimple is firstly formed in the absence of an electric field, the momentum conservation and continuity equations with suitable boundary/initial conditions are used [36,37]. Especially, the fluid flow of a thin deformable film entrapped between the bottom of the droplet and the substrate can be explained by the lubrication theory. Figure 1a presents a schematic of the droplet model. The computational domain is simply described as axisymmetric. The dominant velocity component, $u(r, z, t)$, exists in the radial direction, and the pressure, $p(r, t)$, only varies along the r-direction. The velocity field can be described as the radial component of the Stokes equations [36].

$$\mu \frac{\partial^2 u(r,\ z,\ t)}{\partial z^2} = \frac{\partial p(r,\ t)}{\partial r} \tag{2}$$

The film height, $h(r, t)$, (or interfacial profile beneath droplet) can be obtained by integrating the continuity equation (Equation (3)) from $z = 0$ to $z = h(r, t)$.

$$\frac{1}{r}\frac{\partial}{\partial r}(ru_r) + \frac{\partial u_z}{\partial z} = 0 \tag{3}$$

$$\frac{\partial h(r,\ t)}{\partial t} = -\frac{1}{r}\frac{\partial}{\partial r}\left(r\int_0^{h(r,\ t)} u(r,\ z,\ t)dz\right) \tag{4}$$

$$\left(\because\ u_r = u(r,\ z,\ t),\ u_z = \frac{\partial h(r,\ t)}{\partial t}\right)$$

To integrate this, the boundary conditions at $z = 0$ and $z = h(r, t)$ are required. Various hydrodynamic boundary conditions have been suggested in the references [36–39]. In this analysis, the tangentially immobile boundary condition was utilized, which refers to the no-slip boundary condition. The boundary conditions are as follows.

$$u = 0 \text{ at } z = 0 \text{ and } z = h(r,\ t) \tag{5}$$

Utilizing these boundary conditions, Equation (4) can be described again with the Stokes equation (Equation (2)) as the Stokes-Reynolds equation for thin-film thickness, $h(r, t)$.

$$\frac{\partial h(r,t)}{\partial t} = \frac{1}{12\mu r}\frac{\partial}{\partial r}\left(rh^3\frac{\partial p}{\partial r}\right) \tag{6}$$

where $\partial p/\partial r$ is the pressure gradient.

To get the thin film thickness, $h(r, t)$, the radial pressure gradient ($\partial p/\partial r$) is required. As the droplet approaches the substrate, the pressure beneath the droplet interface increases and the pressure gradient exists from the surrounding gauge pressure. The pressure gradient makes the entrapped air drain outward, and the air film layer becomes thin. Considering those conditions, the pressure in the film is determined by the three components as in Equation (7); a difference of capillary pressure on the droplet (Young-Laplace equation), stagnation pressure at the bottom of the the droplet, and local curvature of droplet interface. The pressure gradient of the air film only exists along the radial direction, and no pressure

gradient exists along the z-direction. Therefore, $p(r,z,t)$ becomes $p(r,t)$. The details of this equation are described in a reference paper [37]. R, σ, ρ, and V_{impact} represent the droplet radius, the surface tension, the density of liquid droplet, and the impact velocity of the droplet, respectively.

$$p(r,\ z,\ t) = p(r,t) = \frac{2\sigma}{R} + \frac{1}{2}\rho\left(V_{\text{impact}}\right)^2 - \frac{\sigma}{2r}\frac{\partial}{\partial r}\left(r\frac{\partial h(r,z)}{\partial r}\right) \tag{7}$$

Equations (6) and (7) are our governing equations for calculating the film thickness and pressure to track the film interface.

- Initial and boundary conditions for tracking film interface

To solve the two governing equations above, we need the initial and boundary conditions for a film profile tracking. The droplet is assumed to be spherical before its dimple formation. Then, the initial condition for the film profile can be represented as [37,38]

$$h = h_0 + \frac{r^2}{2R} \tag{8}$$

The initial velocity of the film is assumed to be the same as the impact velocity because the dimple generally occurs adjacent to the colliding surface. The gauge pressure is assumed to be 0 (ambient pressure) at the end of the film (radial edge of the droplet). Therefore, the boundary conditions are,

$$\frac{\partial h}{\partial t} = -V_{\text{impact}}, \quad p = 0 \ \text{ at } r = R \tag{9}$$

- Nondimensionalization

For nondimensionalization, we utilized the following variables which are composed of the original variables and their relations.

$$p^* = \frac{R}{\sigma}p, \quad t^* = Ca^{1/2}\frac{V_{\text{impact}}}{R}t, \quad r^* = Ca^{1/2}\frac{r}{R}, \quad h^* = Ca^{1/2}\frac{h}{R}, \tag{10}$$

where p^*, t^*, r^*, h^* represents nondimensionalize-pressure, -time, -radius, -film height. Also Ca represents the capillary number $Ca = \left(\mu V_{\text{impact}}/\sigma\right)$. Stokes-Reynolds equation (Equation (6)) and pressure Equation (Equation (7)) were nondimensionalized as follows:

$$\frac{\partial h^*}{\partial t^*} = \frac{1}{12r^*}\frac{\partial}{\partial r^*}\left(r^*h^{*3}\frac{\partial p^*}{\partial r^*}\right) \tag{11}$$

$$p^* = 2 - \frac{R}{\sigma}\left\{\frac{1}{2}\rho\left(V_{\text{impact}}\right)^2\right\} - \left\{\frac{1}{r^*}\frac{\partial}{\partial r^*}\left(r^*\frac{\partial h^*}{\partial r^*}\right)\right\} \tag{12}$$

- Tracking of Film Profiles and Height of Dimple Formation

With the two governing equations and the initial and boundary conditions, the height of the first dimple formation, $h(0,t_{\text{first}})$, was obtained by tracking the film profiles in the absence of electric field. The equations were calculated iteratively with the finite difference method and the Guass-Seidal method [40]. To improve the accuracy, the time step and the distance between nodes were set to 4 ns and 5 μm, respectively. Because the Stokes-Reynolds equations are based on the Stokes regime between the droplet and the substrate, the accuracy of the model for tracking air film profile (Equations (11) and (12)) is limited in the range of relatively low impact velocities. [41] The height of dimple formation and the film profile show good agreement between the model and the experiment only for the low Weber number case. The dripping height for the numerical analysis ranged from 5 to 20 mm, which is same as the experiment. The Weber number (We) for ethanol and DI water was 4.21~24.27 and 0.815~6.20, respectively, which corresponded to the

experimental results (Figure S2). By solving Equations (11) and (12), we could extract the film profile sequentially and the height ($h(0, t_{\text{first}})$) where the dimple was firstly formed due to the increased air pressure. (Figure S3) Table 3 presents the $h(0, t_{\text{first}})$ obtained from the numerical analysis for both ethanol and DI water when no electric field is applied.

Table 3. Dimple formation heights for ethanol and DI water in the absent of an electric field.

Liquid	Dripping Height							
	5 mm		10 mm		15 mm		20 mm	
-	*We*	$h(0, t_{\text{first}})$	*We*	$h(0, t_{\text{first}})$	*We*	$h(0, t_{\text{first}})$	*We*	$h(0, t_{\text{first}})$
-	(-)	(μm)	(-)	(μm)	(-)	(μm)	(-)	(μm)
Ethanol	4.21	5.16	10.41	4.35	17.50	3.44	24.27	4.90
DI water	0.82	3.89	2.57	3.69	4.43	3.44	6.20	3.29

3.1.2. Electrostatic Simulation for Distribution of Electric field

To evaluate the effect of the electric pressure on the suppression, the electric pressure should be calculated at the height of dimple formation, $h(0, t_{\text{first}})$, and then compared with the air film pressure. The distribution of the local electric field and its strength are required to calculate the electric pressure. Therefore, with the charge amount of the droplet (Q_{droplet}, in Tables 1 and 2) by direct measurement (Faraday cup) and the $h(0, t_{\text{first}})$ value, we conducted electrostatic simulation using COMSOL Multiphysics (Finite Element Method, https://www.comsol.kr/multiphysics/finite-element-method, accessed on 1 April 2021).

- Electric Pressure (P_{electric})

Figure 2 depicts the schematic for electrostatic simulation. The electrostatic simulation was conducted based on Gauss's law of Maxwell equations (Equation (14)). Gauss's law states that net electric flux through the closed surface is the same amount of net electric charge within the closed surface. D and ρ_v represent the electric flux intensity and charge density of the control volume. E, V, ε_0, and ε_r represent the electric field strength, electric potential, vacuum permittivity, and relative permittivity, respectively. Zero charge condition was set at the wall boundary to satisfy the charge conservation within all domains (Equation (15)). The droplet was positioned at the height ($h(0, t_{\text{first}})$). DC voltage ($V = V_0$) was applied to the nozzle, and the substrate was grounded ($V = 0$). Also, the surface charge density (ρ_s) was induced on the droplet surface based on the calculated charge amount (Equation (16)). The surface charge density (ρ_s) was calculated based on the charge amount measured in Tables 1 and 2.

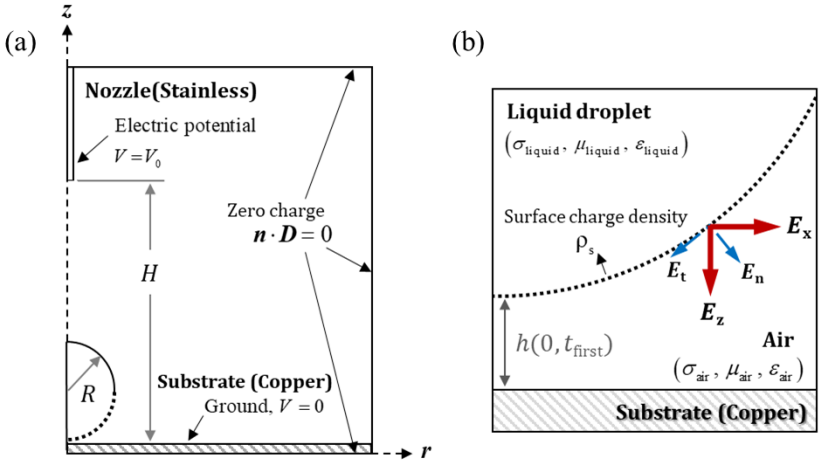

Figure 2. A schematic of boundary conditions for the electrostatic simulation. (**a**) all domain and (**b**) the specified domains nearby the electrified droplet.

The electric field along the liquid surface was divided into the tangential (E_t) and normal (E_n) components. These components can be transformed in the radial and z-directions in the axisymmetric coordinates as shown in (Figure 2b). The radial electric field (E_r) was canceled out as it is axisymmetric. In dimple suppression, we considered the electric field strength toward the z-direction from the droplet surface. Therefore, the z-directional electric field strength (E_z) along the bottom interface of the droplet (dashed line of the droplet in Figure 2) was extracted and the electric pressure was calculated from Equation (1). The external electric field strength (E_0) differs from the z-direction local electric field strength (E_z) on the droplet surface. Figure 3 represents the calculation procedure to achieve the electric pressure.

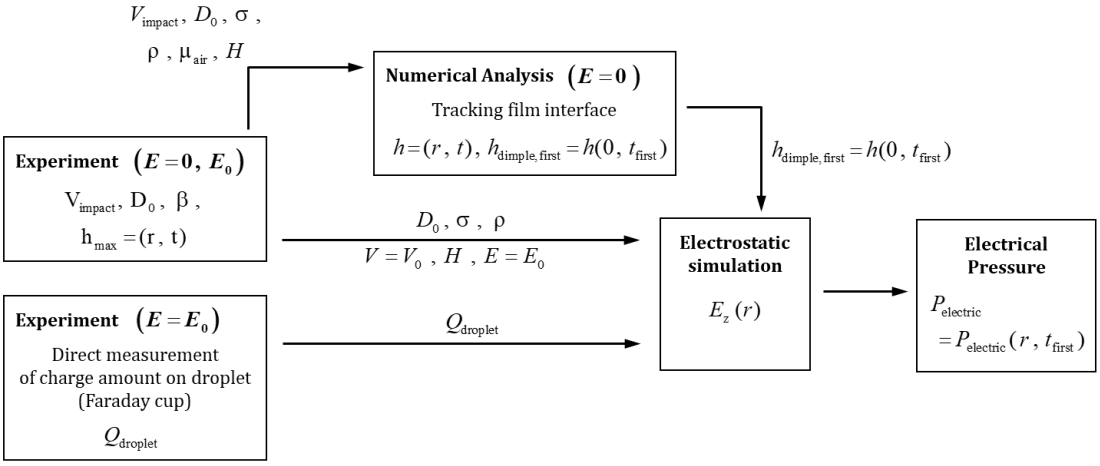

Figure 3. Flow chart to calculate the electric pressure ($P_{electric}$).

$$\nabla \times D = \rho_v \tag{13}$$

$$E = -\nabla V \tag{14a}$$

$$\nabla \times (\varepsilon_0 \varepsilon_r E) = \rho_v \tag{14b}$$

$$n \times D = 0 \tag{15}$$

$$n \times (D_1 - D_2) = \rho_s \tag{16}$$

3.2. Electric Weber Number (We_{elec})

We investigated the relationship between the surface charge on the droplet by the external electric field and the suppression of the air film by utilizing electric Weber number ($We_{elec} = \varepsilon E_0^2 D_0/\sigma$) [42,43]. The electric Weber number is a non-dimensional number describing the ratio of electric force relative to surface tension. σ and D_0 represent the surface tension of the liquid and diameter of the droplet, respectively. In this work, we utilized the electric Weber number as a non-dimensional index to determine certain critical regimes for the electric stress on the suppression of dimple formation.

4. Result and Discussion

4.1. Coalescence Dynamic of Electrified Droplet

We observed different coalescence phenomena of electrified droplets freely falling on dry or wet surfaces. In general, a stepwise cascade coalescence is observed for free-fall droplets to a liquid surface. The 'cascade coalescence' refers to a phenomenon where the droplet coalesces with a liquid surface stepwise. This phenomenon happens because the air film at the interfacial layer intervenes and interrupts the immediate coalescence, with a dimple formation, causing temporal floating and bouncing of the droplet with a staged reduction of the droplet size during coalescence [1,44]. However, in the coalescence of an

electrified droplet on the wet surface, we observed that the stepwise cascade coalescence was suppressed on the wet surface (Video S1). Also, in the coalescence of an electrified droplet on the dry surface, we observed that the thickness of the air film decreases and eventually disappears (Video S2). The 'cascade coalescence' and the observable air film beneath the droplet (interference patterns) are basically related to the dimple formed by pressure inversion. We assumed that the coalescence dynamics under an electric field cause the suppression of dimple formation. Thus, we focused our study on the coalescence dynamics of an electrified droplet on a dry surface.

Figure 4a demonstrates the morphologic characteristics of droplet and air film profiles for the ethanol droplet under various voltages at the moment of impact for the case of the same dripping height, 5 mm. The interference pattern in Figure 4a represents the highest film height, which has appeared among the whole coalescence process. Under 0 V (in the absence of electric field), the free-fall droplet shows a normal spherical shape and the dimple-shaped interface caused by pressure inversion before its collision. The dimple-shaped interface can be clearly confirmed through the interference patterns, which is evidence of density variation beneath the droplet, from the bottom view in Figure 4a. This indicates that air is entrapped due to the dimple formation on the droplet interface. As the applied voltage increased (i.e., the electric field strength increased), the interference ring patterns become small at 100 V and disappear at 300 V. Therefore, an increase in the applied voltage leads to a decrease in the diameter and thickness of the air film. Especially, from a voltage over 200 V, the droplet could collide directly to the substrate without dimple and air film formation. Meanwhile, when the applied voltage reaches 600 V, the bottom of the droplet deforms into a cone shape before the impact, which is an opposite phenomenon to the dimple formation. Detailed images of impact behaviors of the droplet and the changes in the air film's interference pattern are represented in Figure S4. The air film becomes thinner and disappears with an increase of applied voltage, and the shape of the droplet bottom apex becomes sharper like a cone shape. The tendency of interfacial change can be clearly observed from the video taken by a high-speed camera (Video S2). Even for the DI water droplet, the dimple formation was suppressed owing to the applied voltage. (Video S3, Figure S5a)

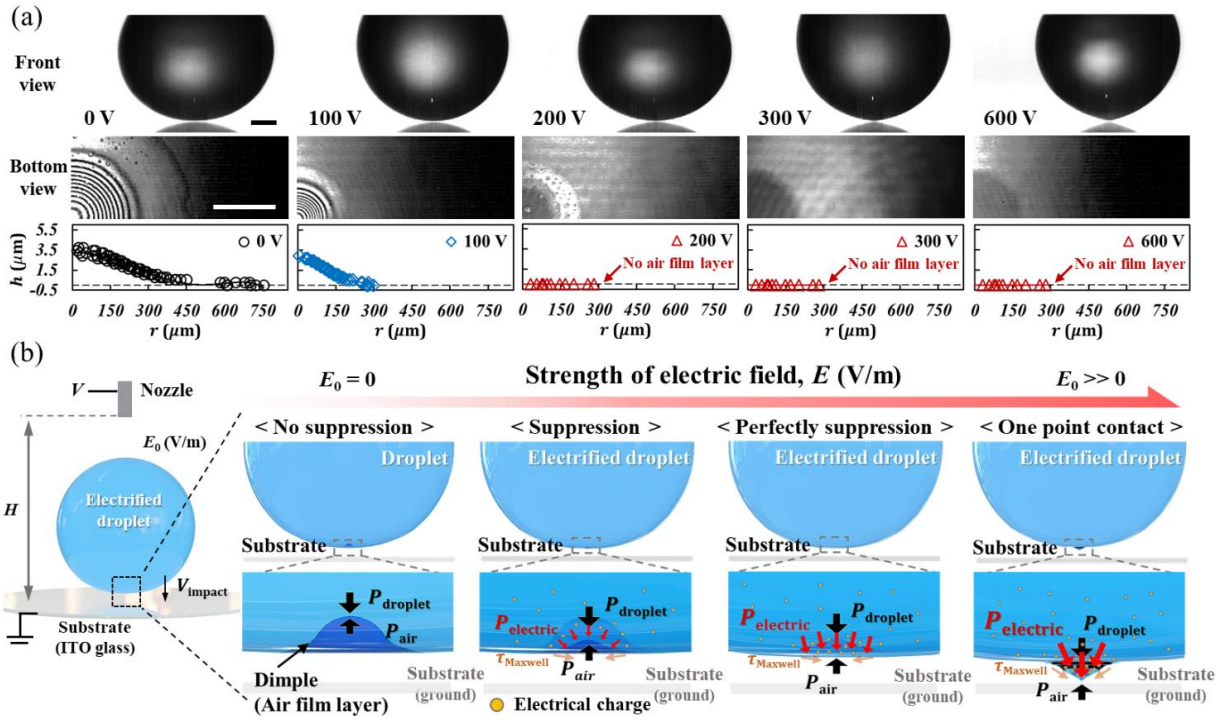

Figure 4. Coalescence dynamics of an electrified droplet under the electric field. (**a**) Front- and bottom-view of the electrified droplet at the colliding moment as the electric field strength increases under the fixed dripping height (5 mm). Scale bars: 300 μm. (**b**) Schematic illustration of the concept of electric pressure affecting to the suppression of dimple formation.

The cone-shaped interfacial morphology was observed between two oppositely colliding charged droplets in a quasi-static condition under an electric field by other researchers [45,46]. However, the previous research studied the interfacial change of two oppositely charged droplets due to the electric field in a dielectric medium, not an air film layer formation and its suppression. Here we report the interfacial morphologic change and the suppression of dimple by the electric field when the electrified droplet collides with the grounded substrate.

To characterize cone-shaped interface's deformation, we measured the contact cone angles (β) between the substrate and droplet while applying various voltages with the same dripping height. (Figure S4) The contact cone angle refers to the instant angle with the substrate when the droplet firstly contacts the substrate. The contact cone angle, which had shown 11° in 300 V, increased to 30° in 1300 V. It clearly demonstrated that the contact cone angle increased proportionally to the magnitude of the applied voltage (the strength of the electric field) (Figures S4 and S5c), which is similar to the reference [47]. It means that the droplet's morphological change under the electric field is caused by electric forces (stress) due to the electrical charge and the electric field. The droplet's diameter and velocity that has changed due to the electric field and electric force might have affected air film suppression in the experiment. We measured the droplet diameters and impact velocities according to the different applied voltages to ensure consistent experimental conditions. There were no considerable changes in droplet diameter and impact velocities even under 0 to 300 V, the range that we clearly observed the effect of the electric field on the suppression. (Figure S5b) It means that the suppression of dimple is not caused by the increase of inertia force (velocity) and the change of surface tension force (droplet diameter) on the droplet. We wanted to evaluate only the electric force's effect on the dimple formation without the change of the inertia (diameter, impact velocity) or change of surface tension on the droplet. Therefore, we could explain the mechanism of the suppression of the air film and the cone-shaped deformation by the effect of electric forces, utilizing the voltage range in 0–300 V.

Figure 4b depicts the schematics of the change of droplet interfaces (dimple formation, suppression of dimple, perfect suppression with the one-point contact by cone-shaped deformation) in the coalescence moment as the voltage is applied. Due to the electric field, the droplet is electrically charged and affected by the electric force. As the droplet approaches the substrate, the electric field is strongly concentrated between the droplet surface and the substrate and provides strong electric stress locally on the charged droplet. The electric stress (Maxwell stress) acts on the surface in a normal direction. This stress affects the local surface tension of the liquid and changes the droplet interface. The electric stress causes the electric pressure, which intends the change the droplet interface. If the electric pressure is stronger than air pressure, it overcomes the pressure inversion and can suppress the dimple formation. Therefore, as electric field strength increases, the electric stress and electric pressure become increase. The droplet would collide to the substrate with the air film suppressed or the interface having cone-shaped deformation.

4.2. Suppression of Dimple of Electrified Droplet

We investigated the thickest profile of the air film layer during the coalescence process through the experimentally obtained interferometry images. We measured the film's maximum thickness, which is the thickness at the center of the droplet ($h_{max} = h(0, t)$). We studied the thickest profile and its maximum thickness of the air film for the various strengths of the electric field on each dripping height. Figure 5a presents the interferometry images for the thickest air film profile and its profile along the radial direction according to the various voltages and the Weber numbers. When the electric field is absent, the radius and the maximum thickness of the air film decreased as the Weber number increased (circle symbol in Figure 5a,b). It notes that the increase of the inertia of droplets (an increase of Weber number) could cause a decrease in the air film thickness. When a voltage was applied and the electrified droplets fell under an electric field, the thickness

of the air film decreased or disappeared even in the low Weber numbers (diamond and triangle symbols in Figure 5a,b). This indicates that the electric pressure has a significant effect on the suppression of the dimple. The suppression of the air film occurs when the effects of electric force are dominant, overcoming the pressure inversion even with low Weber numbers. The overall tendency of the suppression showed similarity for DI water (Figure S6).

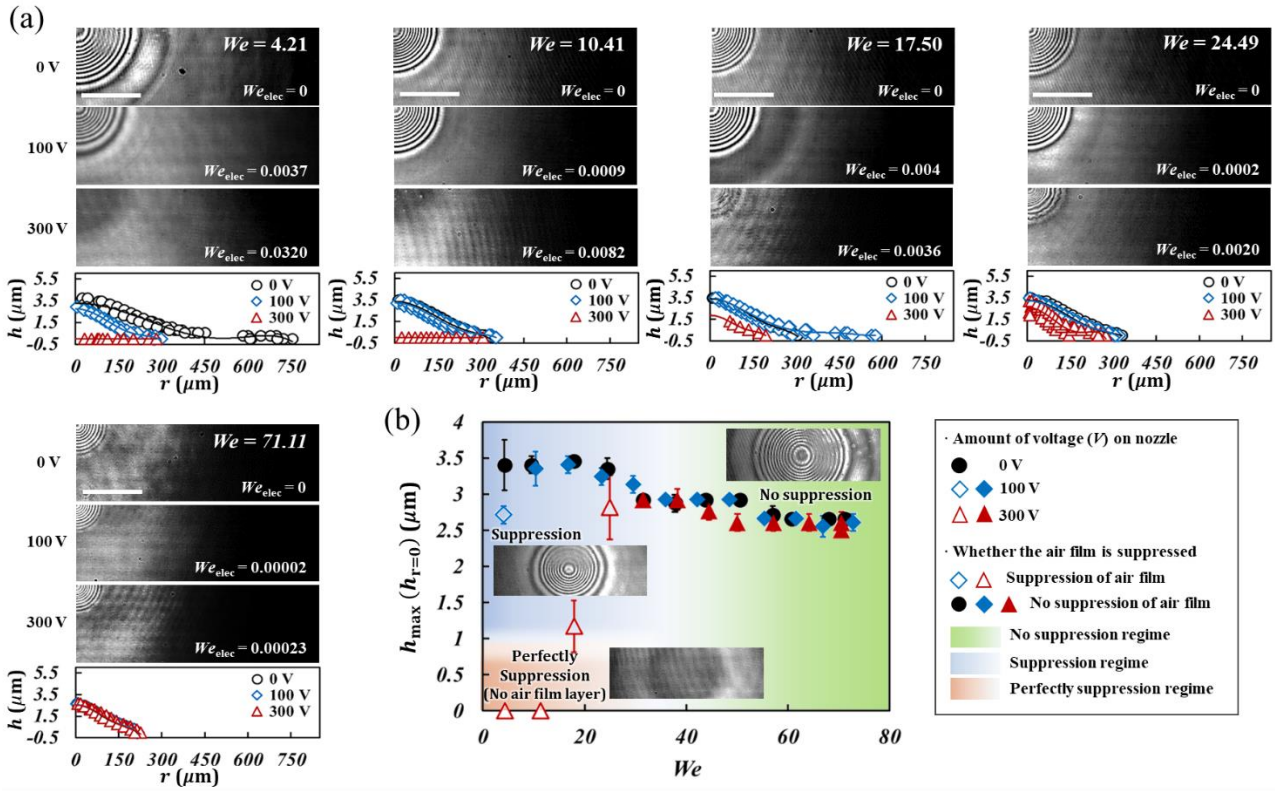

Figure 5. Suppression of the air film layer (or the dimple) for an electrified ethanol droplet under the electric field with respect to various Weber numbers (*We*). (**a**) Snapshots of interferometry observed at the bottom and their corresponding film profiles depending on the amount of applying voltage on each dripping height. (scale bar: 300 μm) The observed film is the maximum film profile ($h_{max} = h(r,\ t_{first})$) which we observed at the beginning of coalescence. (**b**) The maximum film thickness ($h_{max} = h(0,\ t_{first})$) for ethanol droplets based on the Weber number (*We*).

4.3. Electric Pressure in a Coalescence of an Electrified Droplet

We also further investigated the effect of the electric pressure of the droplet by the electric field on the suppression of air film utilizing the electric Weber number ($We_{elec} = \varepsilon {E_0}^2 D_0/\sigma$) [42,43]. The electric Weber number is a non-dimensional number defined by the ratio of the electric force and the surface tension. The surface tension (σ) is a value related to the liquid properties referring to the resistance to its interfacial change and the fast rupture time of the air film. The dielectric constant of liquid (ε), droplet size (D_0), and electric field strength (E_0) in the electric force term are related to the charge amount on the droplet, which causes electric stress on liquid. Figure 6 shows the ratio of the maximum thickness ($h_{max,\ (E_0=E)}/h_{max,\ (E_0=0)}$) depending on the electric Weber number. The ratio was calculated by dividing the maximum film thickness ($h_{max,\ (E_0=E)}$) with the electric field by the maximum film thickness ($h_{max,\ (E_0=0)}$) without the electric field. When the Weber number (electric field strength) is low, the ratio of maximum film thickness almost represents the near of 1 with small variation (inset in Figure 6). This implies that the effect of dimple suppression becomes minor due to the low electric stress. On the other hand, the ratio decreases and becomes 0 as the electric Weber number increases. This implies that the dimple could be successfully suppressed if the electric stress is big enough over a certain critical

value. The suppression of air film occurred when the electric Weber number was more than 0.002 and 0.0035 for ethanol and DI water, respectively (Figure S7a). This indicates that the suppression could occur when the ratio of the electric force and the surface tension is higher than a certain threshold value. Deng and his coworkers suggested the critical level dividing the two regimes regarding whether the droplet contacts the surface in one point without dimple formation [29]. However, the substantive effect of electric stress exists even in the partial suppression of dimples, affecting the coalescence dynamics. Therefore, as investigated in Figure 6, it seems more appropriate to divide the regimes from the point where dimple suppression starts using the electric Weber number.

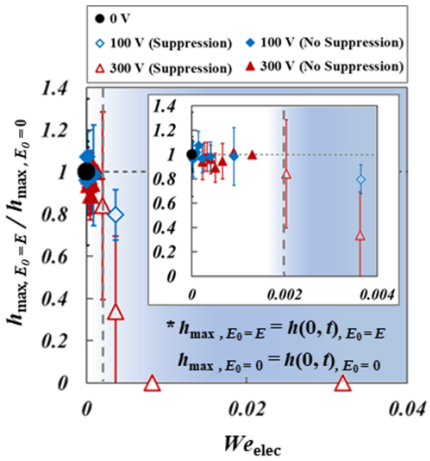

Figure 6. Effects of electric field strength on the suppression of dimple formation. Nondimensionalized film heights based on the electric Weber number (We_{elec}) for an electrified ethanol droplet.

Figure 7a,b represent the strength of the electric field and the amount of electric pressure for the radial location at the bottom interface of the droplet when the applied voltage was 100 and 300 V, respectively. This result is the one obtained above from the numerical tracking for the film interface and the electrostatic simulation. (Equation (1)) The local electric field in Figure 7 is calculated when the droplet was on the height where a dimple firstly occurs. The strength of the electric field shows strongest at the center of the impact area and decreases as it goes to the radial edge of the droplet. The electric pressure also shows the same trend because it is caused by the electric field. The result for DI water also showed the same and it was presented in Figure S7b.

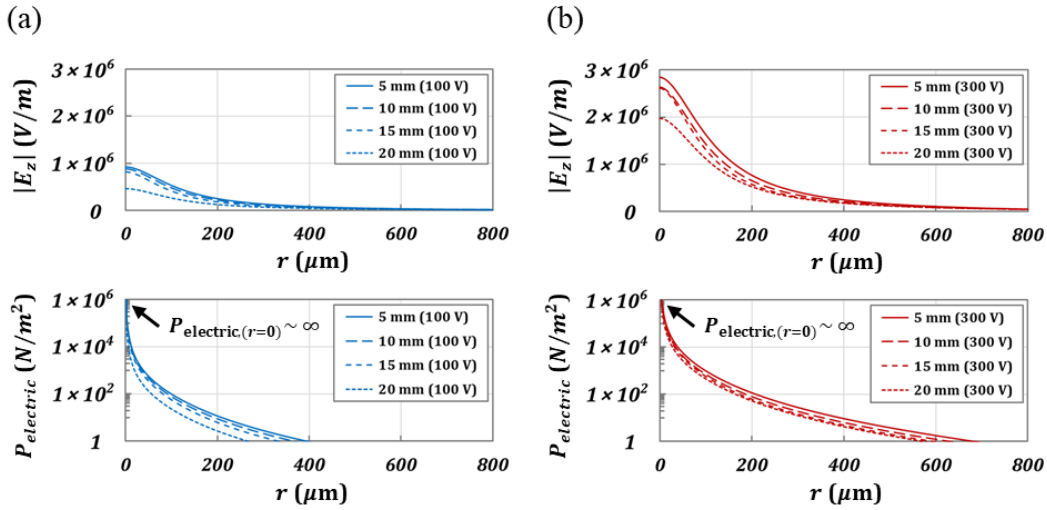

Figure 7. Effects of electric field strength and electric pressure on the suppression of dimple formation. Electric field strength ($|E_z|$) and the strength of electric pressure ($P_{electric}$) with respect to the radial location from the center of coalescence for the electrified ethanol droplet. (**a**) 100 V, (**b**) 300 V (The graph is represented on a logarithmic scale.)

We compared the electric pressure with the air pressure to see whether the electric pressure is enough to suppress the dimple formation. Figure 8a–d depicts the strength of air pressure beneath the droplet and electric pressure acting on a droplet interface. The air pressure and droplet pressure were depicted with one solid black line because they are the same size at the height ($h(0, t_{\text{first}})$) where dimple first occurs. The electrostatic simulation was conducted at the height ($h(0,\ t_{\text{first}})$). The electric pressure was much stronger ($P_{\text{electric}} > h(O^{11})$) than the air film pressure ($P_{\text{air}} < h(O^{3})$) for all 4 Weber number cases. It implies that the dimple can be suppressed enough by the electric force (Figure 5a). DI water also demonstrated that the amount of electric pressure is big enough to overcome the air film pressure for the suppression of dimple (or air film) (Figure S8). It notes that the strength of electric pressure is strong enough to suppress the dimple formation by pressure inversion.

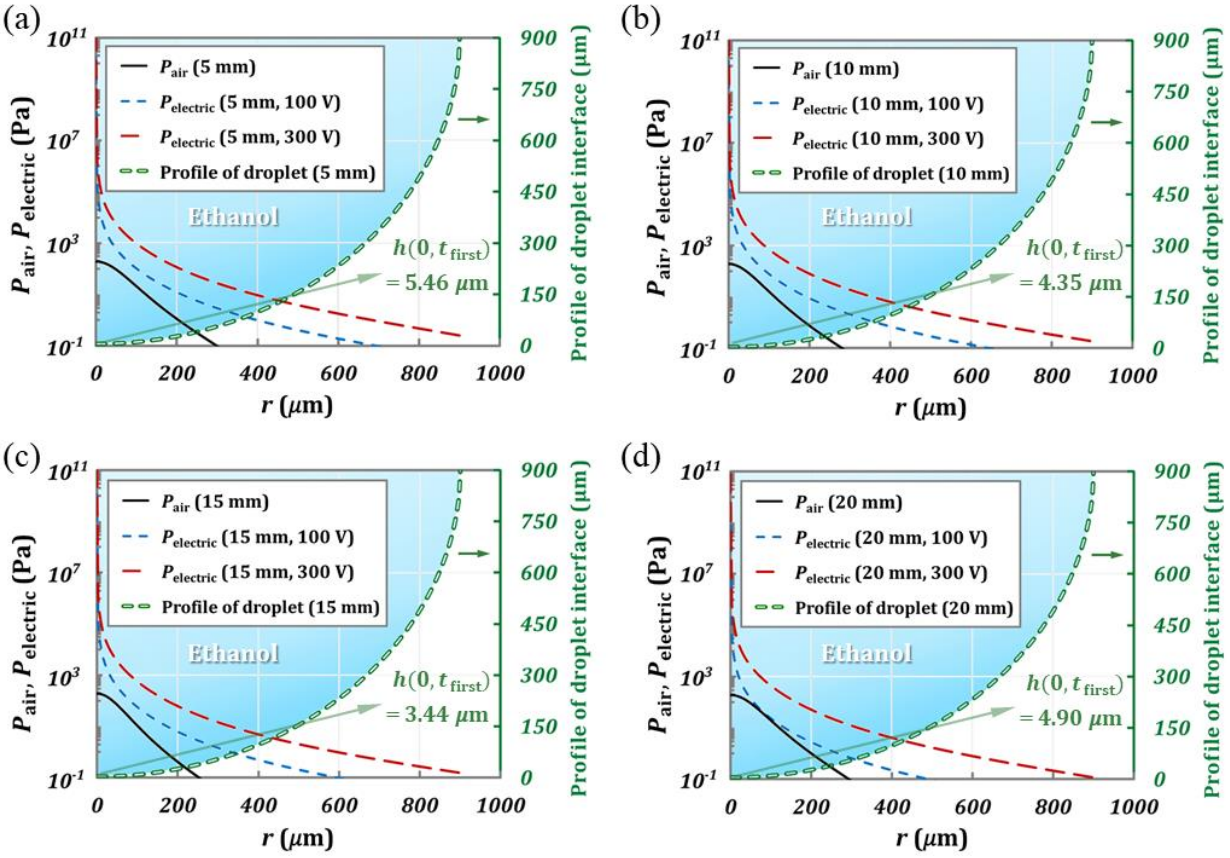

Figure 8. Comparison between electric pressure and the air pressure for an electrified ethanol droplet. (**a**–**d**), Electric pressure and air pressure along the radial direction for electrified ethanol droplet with various applied voltages and 4 Weber numbers (*We* = 4.21, 10.41, 17.50, 24.27).

5. Conclusions

In this work, we observed the coalescence dynamics of an electrified droplet on dry surfaces and elucidated the suppression mechanism for dimple formation based on electric pressure (P_{electric}) and electric Weber number (We_{elec}). When the electrically neutral droplet collides on the dry surface, the droplet interface of the bottom apex is distorted owing to the local pressure inversion, and the dimple with air entrapment occurs. Meanwhile, for the coalescence of an electrified droplet, the bottom interface of the droplet showed the cone-shape distortion, and its shape became more apparent as the strength of the electric field increases. Simultaneously, the dimple's size (height and area) decreased or did not appear even from the moment of coalescence. This unique coalescence behavior could be caused by a free charge on the droplet interface, which distorts the interfacial layer.

We investigated the critical value of electric Weber number that the suppression starts to appear. The dimple started to be suppressed due to electric stress when We_{elec} is over 0.002 and 0.0035 for ethanol and DI water, respectively.

The electric pressure ($P_{electric}$) was introduced as a converted value representing electric stress and to compare it with the air pressure at the bottom of the droplet. $P_{electric}$ was calculated based on the numerical tracking method and electrostatic simulation. The calculated $P_{electric}$ was 10^8 times higher than the air pressure at the center of coalescence, and it showed an exponential decrease along the radial direction. This nonlinear electric stress allows the inverted cone-shaped interfacial change and sequentially enables to overcome the air pressure (suppression of dimple formation).

Supplementary Materials: The following are available online at https://www.mdpi.com/article/10.3390/coatings11050503/s1, Table S1: Experimental conditions, Table S2: Liquid properties in the experiments, Figure S1: Experimental setup, (a) Schematic and (b) Snapshot of the experimental setup, Figure S2: Droplet diameter and impact velocity against dripping height, and Reynolds number (*Re*), Figure S3: Sequential development of air film during the coalescence of droplet and description of $h_{first} = h(0,\ t_{first})$ and h_{max}. h_{first} is the height where a dimple first occurs, and h_{max} is the maximum film height observed in the bottom image of the experimental data, Figure S4: The coalescence dynamics (upper image) and the interferometry (bottom image) of ethanol droplets at the impact moment. The contact cone angle (β) increased with the applied voltage (electric field) on the nozzle. Scale bars: 300 μm, Figure S5: The coalescence dynamics of DI water droplets, and the impact velocity and contact cone angle (β) for DI water and ethanol droplets (a) The coalescence dynamics (top images) and the interferometry (bottom image) of DI water droplets at the impact moment. Scale bars: 300 μm, (b) The change of impact velocity for ethanol and DI water droplets depending on the applied voltage at a fixed dripping height (5 mm), (c) The contact cone angle (β) for ethanol droplets depending on the applied voltage on the nozzle, Figure S6: Suppression of the air film layer (or dimple) of an electrified DI water droplet under the electric field with respect to various Weber numbers (*We*). (a) Snapshots of interferometry observed at the bottom and their corresponding film profiles with respect to the amount of applied voltage on each dripping height. The observed film is the maximum film profile ($h_{max} = h(r,\ t_{first})$) which we observed at the beginning of coalescence. (b) The maximum film thickness ($h_{max} = h(0,\ t_{first})$) of DI water droplets based on the Weber number (*We*), Figure S7: Effects of electric field strength and electric pressure on the suppression of dimple formation. (a) Nondimensionalized film heights based on the electric Weber number (We_{elec}) for an electrified DI water droplet. (b,c) Electric field strength and the strength of electric pressure with respect to the radial location from the center of collision for the electrified DI water droplet. The electric pressure was represented on a logarithmic scale, Figure S8: Comparison between electric pressure and the pressure of air for electrified DI water droplet. (a–d) Electric pressure and pressure of air film along the radial direction of the electrified DI water droplet with respect to various applied voltages under 4 different Weber numbers (*We* = 0.82, 2.57, 4.44, 6.20), Video S1: Cascade Coalescence with different electric field strength, Video S2: Suppression of dimple in a coalescence of electrified ethanol droplet, Video S3: Suppression of dimple in a coalescence of electrified DI water droplet.

Author Contributions: Conceptualization, J.L., B.S. and D.B.; methodology, J.L., G.K. and E.E.; formal analysis, J.L., E.E., S.J. and H.K. (Hosung Kang); resources, D.B.; writing—original draft preparation, J.L.; writing—review and editing, J.K., H.K. (Hyunggun Kim) and D.B.; visualization, J.L. and E.E.; funding acquisition, D.B. All authors have read and agreed to the published version of the manuscript.

Funding: This work was partly supported by the Research and Business Development (R&D) Program of Korea Institute for Advancement of Technology (KIAT) (Grant No. N0002390) and supported by the Basic Science Research Program through the National Research Foundation of Korea (NRF) (Grant No. 2017R1E1A1A01075353).

Institutional Review Board Statement: Not applicable.

Informed Consent Statement: Not applicable.

Data Availability Statement: The data presented in this study are available on request from the corresponding author. The data are not publicly available due to the broad and large amount of data.

Conflicts of Interest: The authors declare no conflict of interest.

References

1. Klyuzhin, I.S.; Ienna, F.; Roeder, B.; Wexler, A.; Pollack, G.H. Persisting water droplets on water surfaces. *J. Phys. Chem. B* **2010**, *114*, 14020–14027. [CrossRef]
2. Chen, L.; Xiao, Z.; Chan, P.C.; Lee, Y.-K.; Li, Z. A comparative study of droplet impact dynamics on a dual-scaled superhydrophobic surface and lotus leaf. *Appl. Surf. Sci.* **2011**, *257*, 8857–8863. [CrossRef]
3. Ju, J.; Bai, H.; Zheng, Y.; Zhao, T.; Fang, R.; Jiang, L. A multi-structural and multi-functional integrated fog collection system in cactus. *Nat. Commun.* **2012**, *3*, 1–6. [CrossRef]
4. Tan, Y.-C.; Ho, Y.L.; Lee, A.P. Droplet coalescence by geometrically mediated flow in microfluidic channels. *Microfluid. Nanofluid.* **2007**, *3*, 495–499. [CrossRef]
5. Christopher, G.; Bergstein, J.; End, N.; Poon, M.; Nguyen, C.; Anna, S.L. Coalescence and splitting of confined droplets at microfluidic junctions. *Lab A Chip* **2009**, *9*, 1102–1109. [CrossRef]
6. Zagnoni, M.; Baroud, C.N.; Cooper, J.M. Electrically initiated upstream coalescence cascade of droplets in a microfluidic flow. *Phys. Rev. E* **2009**, *80*, 046303. [CrossRef]
7. Ihnen, A.C.; Petrock, A.M.; Chou, T.; Fuchs, B.E.; Lee, W.Y. Organic nanocomposite structure tailored by controlling droplet coalescence during inkjet printing. *ACS Appl. Mater. Interfaces* **2012**, *4*, 4691–4699. [CrossRef]
8. Lee, M.W.; Kim, N.Y.; Chandra, S.; Yoon, S.S. Coalescence of sessile droplets of varying viscosities for line printing. *Int. J. Multiph. Flow* **2013**, *56*, 138–148. [CrossRef]
9. Castrejón-Pita, J.; Kubiak, K.; Castrejón-Pita, A.; Wilson, M.; Hutchings, I.M. Mixing and internal dynamics of droplets impacting and coalescing on a solid surface. *Phys. Rev. E* **2013**, *88*, 023023. [CrossRef]
10. Yang, X.; Chhasatia, V.H.; Sun, Y. Oscillation and recoil of single and consecutively printed droplets. *Langmuir* **2013**, *29*, 2185–2192. [CrossRef]
11. Sarojini KG, K.; Dhar, P.; Varughese, S.; Das, S.K. Coalescence dynamics of PEDOT:PSS droplets impacting at offset on substrates for inkjet printing. *Langmuir* **2016**, *32*, 5838–5851. [CrossRef]
12. Cao, X.; Ye, Y.; Tang, Q.; Chen, E.; Jiang, Z.; Pan, J.; Guo, T. Numerical analysis of droplets from multinozzle inkjet printing. *J. Phys. Chem. Lett.* **2020**, *11*, 8442–8450. [CrossRef] [PubMed]
13. Ko, G.H.; Ryou, H.S. Droplet collision processes in an inter-spray impingement system. *J. Aerosol Sci.* **2005**, *36*, 1300–1321. [CrossRef]
14. Kim, S.; Lee, D.J.; Lee, C.S. Modeling of binary droplet collisions for application to inter-impingement sprays. *Int. J. Multiph. Flow* **2009**, *35*, 533–549. [CrossRef]
15. Damak, M.; Mahmoudi, S.R.; Hyder, M.N.; Varanasi, K.K. Enhancing droplet deposition through in-situ precipitation. *Nat. Commun.* **2016**, *7*, 1–9. [CrossRef] [PubMed]
16. Finotello, G.; Padding, J.T.; Deen, N.G.; Jongsma, A.; Innings, F.; Kuipers, J. Effect of viscosity on droplet-droplet collisional interaction. *Phys. Fluids* **2017**, *29*, 067102. [CrossRef]
17. Li, E.; Vakarelski, I.U.; Thoroddsen, S.T. Probing the nanoscale: The first contact of an impacting drop. *J. Fluid Mech.* **2015**, *785*. [CrossRef]
18. Josserand, C.; Thoroddsen, S.T. Drop impact on a solid surface. *Annu. Rev. Fluid Mech.* **2016**, *48*, 365–391. [CrossRef]
19. De Ruiter, J.; Lagraauw, R.; Van Den Ende, D.; Mugele, F. Wettability-independent bouncing on flat surfaces mediated by thin air films. *Nat. Phys.* **2015**, *11*, 48. [CrossRef]
20. Ding, Z.; Xing, R.; Fu, Q.; Ma, D.; Han, Y. Patterning of pinhole free small molecular organic light-emitting films by ink-jet printing. *Org. Electron.* **2011**, *12*, 703–709. [CrossRef]
21. Saha, J.K.; Bukke, R.N.; Mude, N.N.; Jang, J. Significant improvement of spray pyrolyzed ZnO thin film by precursor optimization for high mobility thin film transistors. *Sci. Rep.* **2020**, *10*, 1–11. [CrossRef] [PubMed]
22. Meng, J.; Lau, C.H.; Xue, Y.; Zhang, R.; Cao, B.; Li, P. Compatibilizing hydrophilic and hydrophobic polymers via spray coating for desalination. *J. Mater. Chem. A* **2020**, *8*, 8462–8468. [CrossRef]
23. Seong, B.; Hwang, S.; Jang, H.-S.; Lee, H.; Kim, J.; Nguyen, V.D.; Cho, D.-H.; Lin, L.; Byun, D. A hybrid aerodynamic and electrostatic atomization system for enhanced uniformity of thin film. *J. Electrost.* **2017**, *87*, 93–101. [CrossRef]
24. Qin, H.; Wei, C.; Dong, J.; Lee, Y.-S. Direct printing and electrical characterization of conductive micro-silver tracks by alternating current-pulse modulated electrohydrodynamic jet printing. *J. Manuf. Sci. Eng.* **2017**, *139*, 021008. [CrossRef]
25. Shin, D.-Y.; Yoo, S.-S.; Song, H.-e.; Tak, H.; Byun, D. Electrostatic-force-assisted dispensing printing to construct high-aspect-ratio of 0.79 electrodes on a textured surface with improved adhesion and contact resistivity. *Sci. Rep.* **2015**, *5*, 16704. [CrossRef] [PubMed]
26. Lee, H.; Seong, B.; Kim, J.; Jang, Y.; Byun, D. Direct alignment and patterning of silver nanowires by electrohydrodynamic jet printing. *Small* **2014**, *10*, 3918–3922. [CrossRef]
27. Seong, B.; Chae, I.; Lee, H.; Nguyen, V.D.; Byun, D. Spontaneous self-welding of silver nanowire networks. *Phys. Chem. Chem. Phys.* **2015**, *17*, 7629–7633. [CrossRef]
28. Guo, Q.; Mather, J.P.; Yang, P.; Boden, M.; Mather, P.T. Fabrication of polymeric coatings with controlled microtopographies using an electrospraying technique. *PLoS ONE* **2015**, *10*, e0129960. [CrossRef]

29. Gao, F.; Yi, H.; Qi, L.; Qiao, R.; Deng, W. Weakly charged droplets fundamentally change impact dynamics on flat surfaces. *Soft Matter* **2019**, *15*, 5548–5553. [CrossRef]
30. Bouwhuis, W.; Van der Veen, R.C.; Tran, T.; Keij, D.L.; Winkels, K.G.; Peters, I.R.; Van der Meer, D.; Sun, C.; Snoeijer, J.H.; Lohse, D. Maximal air bubble entrainment at liquid-drop impact. *Phys. Rev. Lett.* **2012**, *109*, 264501. [CrossRef]
31. Mehdi-Nejad, V.; Mostaghimi, J.; Chandra, S. Air bubble entrapment under an impacting droplet. *Phys. Fluids* **2003**, *15*, 173–183. [CrossRef]
32. San Lee, J.; Weon, B.M.; Je, J.H.; Fezzaa, K. How does an air film evolve into a bubble during drop impact? *Phys. Rev. Lett.* **2012**, *109*, 204501.
33. De Ruiter, J.; Oh, J.M.; Van den Ende, D.; Mugele, F. Dynamics of collapse of air films in drop impact. *Phys. Rev. Lett.* **2012**, *108*, 074505. [CrossRef]
34. Choi, D.; Lee, H.; Kang, I.S.; Lim, G.; Kim, D.S.; Kang, K.H. Spontaneous electrical charging of droplets by conventional pipetting. *Sci. Rep.* **2013**, *3*, 2037. [CrossRef]
35. Lee, H.; Choi, D.; Kim, D.S.; Lim, G. Capacitive control of spontaneously induced electrical charge of droplet by electric field-assisted pipetting. *Nano-Micro Lett.* **2015**, *7*, 341–346. [CrossRef] [PubMed]
36. Chan, D.Y.; Klaseboer, E.; Manica, R. Theory of non-equilibrium force measurements involving deformable drops and bubbles. *Adv. Colloid Interface Sci.* **2011**, *165*, 70–90. [CrossRef]
37. Klaseboer, E.; Manica, R.; Chan, D.Y. Universal behavior of the initial stage of drop impact. *Phys. Rev. Lett.* **2014**, *113*, 194501. [CrossRef]
38. Lee, S.; Denn, M.; Crochet, M.; Metzner, A. Compressive flow between parallel disks:: I. Newtonian fluid with a transverse viscosity gradient. *J. Non-Newton. Fluid Mech.* **1982**, *10*, 3–30. [CrossRef]
39. Klaseboer, E.; Chevaillier, J.P.; Gourdon, C.; Masbernat, O. Film drainage between colliding drops at constant approach velocity: Experiments and modeling. *J. Colloid Interface Sci.* **2000**, *229*, 274–285. [CrossRef]
40. De Ruiter, J.; Van den Ende, D.; Mugele, F. Air cushioning in droplet impact. II. Experimental characterization of the air film evolution. *Phys. Fluids* **2015**, *27*, 012105. [CrossRef]
41. Hendrix, M.H.; Bouwhuis, W.; Van der Meer, D.; Lohse, D.; Snoeijer, J.H. Universal mechanism for air entrainment during liquid impact. *J. Fluid Mech.* **2016**, *789*, 708–725. [CrossRef]
42. Eow, J.S.; Ghadiri, M.; Sharif, A. Deformation and break-up of aqueous drops in dielectric liquids in high electric fields. *J. Electrost.* **2001**, *51*, 463–469. [CrossRef]
43. Mousavichoubeh, M.; Shariaty-Niassar, M.; Ghadiri, M. The effect of interfacial tension on secondary drop formation in electro-coalescence of water droplets in oil. *Chem. Eng. Sci.* **2011**, *66*, 5330–5337. [CrossRef]
44. Thoroddsen, S.; Takehara, K. The coalescence cascade of a drop. *Phys. Fluids* **2000**, *12*, 1265–1267. [CrossRef]
45. Ristenpart, W.; Bird, J.; Belmonte, A.; Dollar, F.; Stone, H. Non-coalescence of oppositely charged drops. *Nature* **2009**, *461*, 377. [CrossRef]
46. Wang, J.; Wang, B.; Qiu, H. Coalescence and breakup of oppositely charged droplets. *Sci. Rep.* **2014**, *4*, 7123. [CrossRef] [PubMed]
47. Bird, J.C.; Ristenpart, W.D.; Belmonte, A.; Stone, H.A. Critical angle for electrically driven coalescence of two conical droplets. *Phys. Rev. Lett.* **2009**, *103*, 164502. [CrossRef]